PROCEEDINGS OF SCIENCE

MeV-GeV polarimetry with the *Fermi*-LAT

Adrien Laviron,[a,*] **Denis Bernard**[a] **and Philippe Bruel**[a] **for the *Fermi*-LAT collaboration**

[a] *Laboratoire Leprince-Ringuet, CNRS/IN2P3, Ecole polytechnique, Institut Polytechnique de Paris, 91120 Palaiseau, France*

E-mail: adrien.laviron@llr.in2p3.fr

A measurement of MeV-GeV linear polarization would provide information about the emission mechanisms of gamma-ray sources, especially pulsars and AGN (Active Galaxy Nuclei). The *Fermi* Large Area Telescope (*Fermi*-LAT) detects gamma rays between 20 MeV and ∼300 GeV, using their conversion into an electron-positron pair, with the linear polarization affecting the azimuthal direction of the pair. Measuring this azimuthal direction is extremely challenging due to the multiple scattering of the electron-positron pair in the detector. We present the current effort to extract the polarization information from the *Fermi*-LAT data, including recent developments in the simulation implementation and the event reconstruction and selection. This allows us to estimate the expected sensitivity to linear polarization of the *Fermi*-LAT, and we apply this to the Vela pulsar.

38th International Cosmic Ray Conference (ICRC2023)
26 July - 3 August, 2023
Nagoya, Japan

*Speaker

PoS(ICRC2023)721

1. Introduction

Pulsars were discovered in 1967 as pulsating radio sources. They were quickly interpreted as magnetized, rotating neutron stars. Pulsars are well-known gamma-ray sources, with 294 of them detected by the *Fermi*-LAT since 2008 in the 100 MeV – 300 GeV energy range[1], whose gamma-ray emission has a spectral shape of a power-law with sub-exponential cutoff at an energy of a few GeV [1].

If the radio emission is thought to originate from the polar cap, the gamma-ray emission cannot escape that part of the magnetosphere because of $\gamma + \overrightarrow{B} \rightarrow e^+ + e^-$ conversion induced by the intense magnetic field [2]. The gamma-ray emission therefore comes from an outer part of the magnetosphere, but the exact location of that emission region and the radiative process at play are still debated. The polarization signature of these different emission processes and emission regions differ significantly [3], with curvature radiation emitted within the light cylinder thought to be more polarized than synchrotron emission from the striped wind.

In the MeV to GeV energy range, the dominant interaction process of gamma rays with matter is $e^+ - e^-$ pair production. This process is inherently sensitive to linear polarization: the bisector φ of the azimuthal angles of the electron and positron is preferentially perpendicular to the polarization direction, as can be seen in Figure 1 (left).

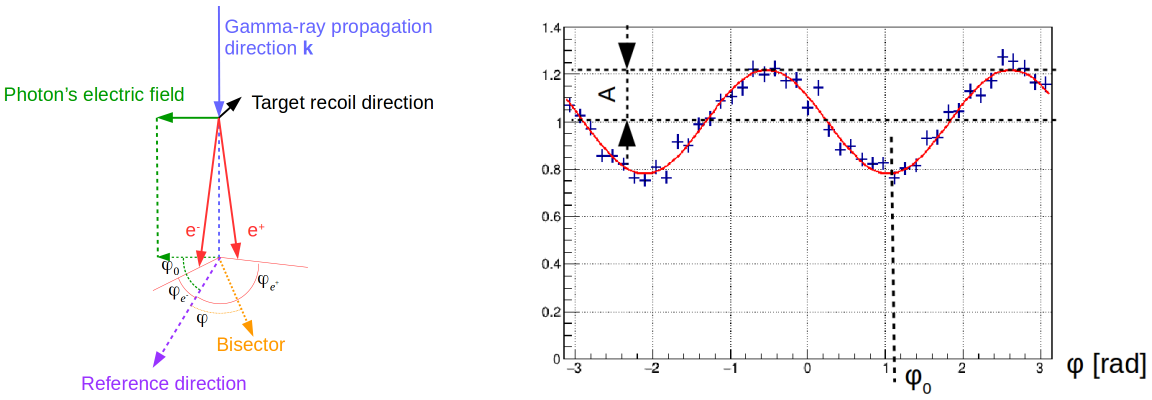

Figure 1: Left: diagram of pair production. Right: distribution of φ angles, called a polarigram. The distribution minimum φ_0 is the polarization angle, the amplitude A is related to the polarization fraction.

We compute φ as

$$\varphi = \frac{\varphi_{e^-} + \varphi_{e^+}}{2} \ , \tag{1}$$

where φ_{e^-} (resp. φ_{e^+}) is the angle between the momentum of the electron (resp. positron) and a reference direction in the plane perpendicular to the photon direction. In the following, the reference direction will be that of the celestial north pole, with angles computed North to East, as it is the standard in polarimetric astronomical observations (see [4] and

[1] https://confluence.slac.stanford.edu/display/GLAMCOG/Public+List+of+LAT-Detected+Gamma-Ray+Pulsars

refs. therein). We note here that computing φ does not require distinguishing the electron from the positron, as inverting the two does not affect the computed value of φ.

The φ distribution, called in the following "polarigram", therefore has a cosine modulation, as can be seen on Figure 1 (right). One of the minima of the polarigram is the polarization angle φ_0 and the amplitude of the modulation A is proportional to the polarization fraction Π.

$$\Pi = \frac{A}{A_{100}} \ , \tag{2}$$

where A_{100} is the modulation of a 100 % polarized source.

The *Fermi*-LAT [5] is a gamma-ray space telescope, using pair production and observing in the 20 MeV to $\gtrsim$ 300 GeV energy range. It is composed of three main subsystems: a tracker to measure the direction of the incoming gamma ray, a calorimeter to measure its energy, and an anti-coïncidence detector (ACD) to reject charged cosmic rays.

The LAT was designed to optimize the effective area and angular resolution throughout its energy range, but not its polarization sensitivity. Previous polarimetry attempts using information provided by the standard *Fermi*-LAT reconstruction were not successful [6].

Here we present a new approach to *Fermi*-LAT polarimetry based on the work of [7]. It requires a dedicated event reconstruction and selection that is described in Section 2. Section 3 presents the results and a preliminary polarization sensitivity estimate applied to the Vela pulsar.

To develop this method, we performed Monte-Carlo simulations of gamma rays in the LAT detector using Gleam [5], a simulation software based on the Geant4 toolkit [8]. The physics list of the Geant4 simulation has been modified to use the recent 5-dimensional, polarized Bethe-Heitler gamma-ray conversion model [9].

2. Methodology

2.1 Standard event reconstruction

The tracker is composed of 4×4 towers. Each tower contains 18 detector layers, each layer being composed of two single-sided silicon strip detectors, one dedicated to the measurement of the x coordinate and the other to the y coordinate[2]. For that purpose, they are electrically segmented along one direction with strips separated by 0.228 mm. The top 12 layers have a thin tungsten converter (3.5 % radiation length, 0.1 mm) and compose the *Front* section of the tracker. The *Back* section of the tracker consists of 4 layers with a thick tungsten converter (18 % radiation length, 0.72 mm).

The *Fermi*-LAT standard event reconstruction algorithm (named Pass 8 [10]) first groups contiguous strips that triggered into clusters in each silicon plane. Then it combines clusters to form tracks that are fitted to extract their direction. Next, it chooses the best

[2] The LAT frame is cartesian, with the x and y coordinates spanning the silicon detectors plane, and the z coordinate pointing towards the LAT boresight.

track, that we call "the Pass 8 track" in the following, to reconstruct the incident gamma-ray direction. The starting point of the Pass 8 track provides the reconstructed conversion point.

2.2 Azimuthal angle reconstruction

The main challenge in pair-production polarimetry is the multiple Coulomb scattering of the electron and positron by the detector material, especially near the gamma-ray conversion point. Multiple scattering increases with the amount of material crossed. Therefore, as was found in [7], the azimuthal angle can be computed from the first two layers of the event, the conversion layer and in the layer just below the conversion layer, called hereafter the "layer below conversion".

Using the Monte-Carlo simulations, we looked at the clusters that are associated to the $e^+ - e^-$ pair and around the Pass 8 track. We found that the clusters that are within 1 mm of the reconstructed gamma-ray track in the conversion layer, and within 10 mm in the layer below conversion are mostly associated to the pair, so we decided to discard the other ones.

In order to compute a pair azimuthal angle from the cluster information, we need one point in the conversion layer, and two points (corresponding to the crossing points of the electron and positron) in the layer below conversion. We select events that have at least one cluster (in either x or y) and at most one cluster in x and one cluster in y in the conversion layer. For events that only have one cluster in the conversion layer, we assume that the gamma ray comes from the source and we compute the missing coordinate by projecting the coordinates of the clusters in the layer below conversion into the conversion layer.

In the layer below conversion, we use events that have two clusters in either x or y and either one or two clusters in the other direction. This leads to two configurations that are shown in Figure 2. We name them according to their number of possible azimuthal angles (NPAA). The one schematized on Figure 2 (left) is called NPAA1. It has two x coordinates for the electron and positron and a single y coordinate, leaving a single possible pair azimuthal angle, computed using the coordinates in the conversion layer and the two xy coordinates indicated by black triangles. An event with two selected clusters in y and a single cluster in x would be classified as NPAA1 as well and its azimuthal angle calculated in a similar way. The event category shown on Figure 2 (right) has two x coordinates and two y coordinates. This results in an ambiguity: we could compute an azimuthal angle using either the two coordinates indicated by the black triangles or by the black squares. We therefore call these events NPAA2. In that case, we use the azimuthal angle computed from the pair possibility that is closer to the Pass 8 track.

2.3 Event selection

Since we want to measure the polarization of a given gamma-ray source, we only consider Pass 8 SOURCE events whose angular separation from the source direction is less than the PSF 95 % containment radius.

To maximize the polarimetric information, we want to select events for which the reconstructed conversion point is close to the actual conversion point. The simulation

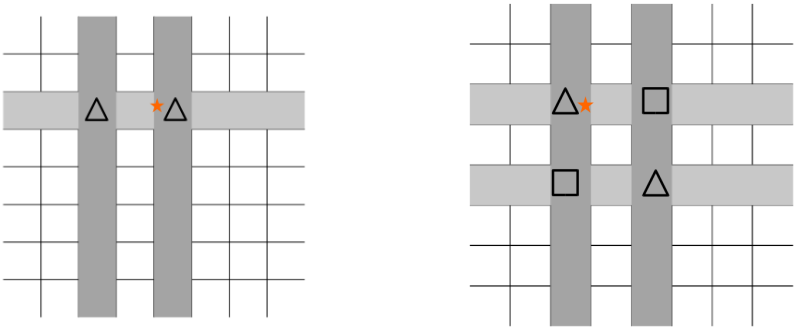

Figure 2: Cluster configurations in the layer below conversion. Light grey represents the y clusters and dark grey the x clusters. The orange star represents the coordinates of the Pass 8 track in that plane. The black triangles and squares represent the sets of (x, y) positions that we may use to compute an azimuthal angle. Left: NPAA1 category (there is one cluster in either x or y). Right: NPAA2 category (there are two clusters in both x and y, yielding two possible azimuthal angles).

shows that for most of the events the distance is less than 1 mm. The events with a larger distance mostly correspond to events that convert in the dead material between towers and whose conversion point is reconstructed close to the tower edge. In order to reject these events, we require that the Pass 8 track trajectory between the layers above and below the conversion layer is contained in one tower and that the distances of the Pass 8 track to the tower edge in the layers above and below the conversion layer are larger than 20 mm and 30 mm, respectively.

We also reject events whose conversion point is reconstructed in the top silicon detector of the top layer of the tracker, because these events were found to be $\sim 45\,\%$ converted outside the LAT sensitive volume at 100 MeV, mostly in the structural material of the ACD.

2.4 Event categories

As demonstrated in [7], it is useful to classify the events into categories that carry different levels of polarimetric information, because of different levels of multiple scattering. Given the LAT geometry, the usual and most obvious categorization depends on whether the gamma ray converted into the Front or Back section of the tracker.

Within the detector layer, the conversion happens either in the silicon detectors or in the tungsten converter, where multiple scattering is greater. By construction, the Pass 8 reconstructed z conversion coordinate is located in either the upper or lower silicon detector of the conversion layer. At 100 MeV, 5.6 % of the events hor which conversion is located in the upper silicon detector, called hereafter "upper detector" events, converted in silicon, the rest mostly converted in tungsten. On the contrary, 76 % of the events for which conversion is located in the lower silicon detector ("lower detector" events) converted in silicon. The high fraction of tungsten conversion in "upper detector" events makes them less sensitive to polarization. "Lower detector" events represent only 5.5 % of all selected events at 100 MeV, but their much higher silicon conversion fraction makes them much more sensitive to polarization.

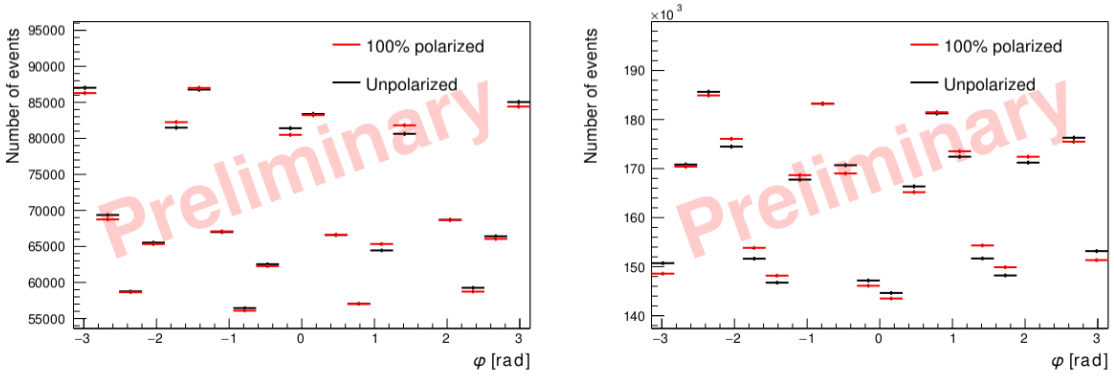

Figure 3: Distribution of φ azimuthal angles, for a 100 % polarized source in red and a 0 % polarized source in black. Only Front-converted and upper detector events are shown. Left: distribution for NPAA1 events. Right: NPAA2 events.

Thus, each event is either Front or Back, and either "upper detector" or "lower detector", and either NPAA1 or NPAA2. We define the event categories as the set $\{\text{Front}, \text{Back}\} \times \{\text{upper}, \text{lower}\} \times \{\text{NPAA1}, \text{NPAA2}\} \times \{\text{Energy}\}$, and the category of the event as its tuple in that set, e.g. (Front, upper, NPAA2, 100 MeV).

3. Results

In order to estimate the *Fermi*-LAT sensitivity to polarization, we first measure the modulation amplitude A_{100} (defined in Eq. 2) for each event category. To do so, we simulated gamma rays from the celestial coordinates of the Vela pulsar (R.A. = 128.84 °, Dec = −45.18 °). Their polarization direction is set with respect to the celestial north pole (R.A. = 0 °, Dec = 90 °). These directions are then converted to the frame of the spacecraft, in which the simulation is run. We set the simulation to span a time of ∼ 55 days, corresponding to a full precession period of the satellite. The attitude of the satellite (its orientation in space) is that of the actual spacecraft in the time range 2012-09-28 00:06:00 to 2012-11-22 02:09:20. This time range was chosen because it is representative of the attitude of the spacecraft during the whole mission, with a rocking angle of 50 °.

Simulations were performed at three energies: 50 MeV, 100 MeV and 200 MeV. For each energy, we simulated an unpolarized source (0 % polarized), and a fully polarized source (100 % polarized, polarization angle of 0 ° with respect to the celestial north pole).

Figure 3 shows examples of polarigrams, for 100 MeV, Front-converted and upper detector converted, NPAA1 events (left) and NPAA2 events (right). These distributions do not show the cosine modulation because they are dominated by the x-y structure of the detector segmentation of the LAT tracker.

Ratios (bin-to-bin) of the polarized distribution to the unpolarized distribution are shown on Figure 4. For simplicity's sake, we refer to these ratios as polarigrams. We fit these ratios with a cosine function to extract the modulation amplitudes A_{100}. The amplitudes of Front, upper detector events are 0.77 ± 0.16 % for NPAA1 events and $1.20 \pm$

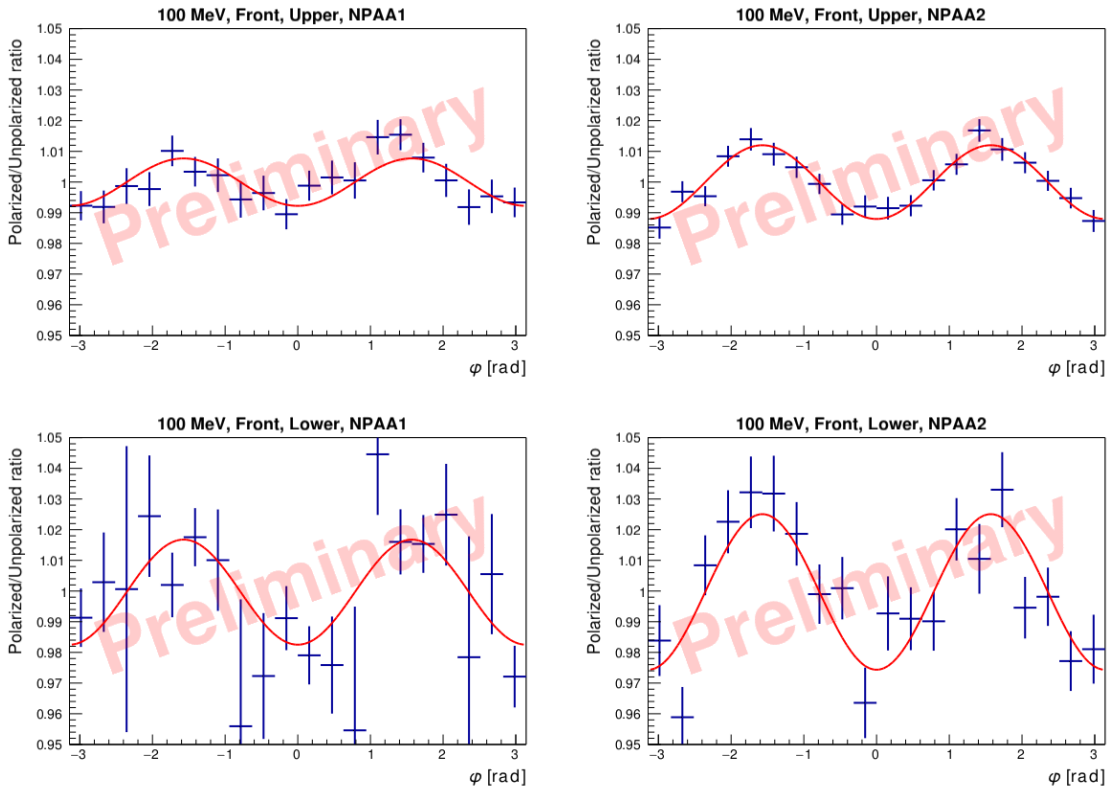

Figure 4: Polarigrams of Front events at 100 MeV. Top: "upper detector" events. Bottom: "lower detector" events. Left: NPAA1. Right: NPAA2.

0.11 % for NPAA2 events (respectively 1.72 ± 0.35 % and 2.54 ± 0.35 % for Front, lower detector events). We observe that modulations of NPAA1 events are smaller than those of NPAA2 events, because the azimuthal angles reconstructed in NPAA1 events are less precise. We also see that, as expected, the "lower detector" events are much more sensitive to polarization. Finally, the modulation of Back events (not shown here) is compatible with zero for most categories. These overall low numbers confirm that the LAT was not designed for polarimetry. The modulation amplitudes vary slightly with energy. All these results are comparable to those obtained with a simplified model of the *Fermi*-LAT in [7].

In order to maximize the statistical significance of the measurement combining event categories, we weight events according to A_k and N_k, the A_{100} value and number of events in category k [7]. Event categories that have a modulation A_{100} compatible with zero are discarded. The resulting uncertainty on the measured linear polarization fraction σ_P is

$$\sigma_\mathrm{P} = \frac{W}{\sqrt{\sum_{k\in\{\text{Event categories}\}} N_k A_k^2}} \,, \tag{3}$$

where $W \simeq \sqrt{2}$ and the event category is defined in Section 2.4 as a tuple in the space $\{\text{Front}, \text{Back}\} \times \{\text{upper}, \text{lower}\} \times \{\text{NPAA1}, \text{NPAA2}\} \times \{\text{Energy}\}$, e.g. (Front, lower, NPAA1, 50 MeV).

Our simulations at 50 MeV, 100 MeV and 200 MeV are at the center of three logarithmic energy bins in the range 35 MeV to 283 MeV. In that energy range, the observed Vela pulsar count spectrum is almost flat, and the expected number of photons is $\sim 2 \times 10^6$ for 15 years of observation. Applying Eq. 3 to our data, we get $\sigma_{\mathrm{P}} \simeq 20\,\%$.

4. Conclusions

We have presented a new analysis that allows us to obtain for the first time a non-zero sensitivity to linear polarization with Fermi-LAT. This result is enabled by directly using the tracker cluster information rather than the output of the standard event reconstruction. Using simulations, we measure modulation amplitudes up to 2.5 % in the energy range between 30 and 300 MeV and estimate the expected sensitivity to the linear polarization of the Vela pulsar to about 20 % with 15 years of data. The next step of this study is to simulate more photons to improve the precision of the modulation amplitudes and to extend the energy range. We will then apply the analysis to *Fermi*-LAT data.

Acknowledgements

The *Fermi*-LAT Collaboration acknowledges support for LAT development, operation and data analysis from NASA and DOE (United States), CEA/Irfu and IN2P3/CNRS (France), ASI and INFN (Italy), MEXT, KEK, and JAXA (Japan), and the K.A. Wallenberg Foundation, the Swedish Research Council and the National Space Board (Sweden). Science analysis support in the operations phase from INAF (Italy) and CNES (France) is also gratefully acknowledged. This work performed in part under DOE Contract DE-AC02-76SF00515.

References

[1] Smith et al. ApJ Supplement Series submitted (2023).

[2] Abdo, A. A., Ackermann, M., Ajello, M., et al. 2010, ApJ Supplement Series, 187, 460.

[3] Harding, A. K. & Kalapotharakos, C. 2017, ApJ, 840, 73.

[4] Hamaker, J. P. & Bregman, J. D. 1996, A&A Supplement Series, 117, 161

[5] Atwood, W. B., Abdo, A. A., Ackermann, M., et al. 2009, ApJ, 697, 1071.

[6] Giomi, M., Bühler, R., Sgrò, C., et al. 2017, 6th International Symposium on High Energy Gamma-Ray Astronomy, 1792, 070022.

[7] Bernard, D. 2022, NIMPA, 1042, 167462.

[8] Agostinelli, S., Allison, J., Amako, K., et al. 2003, NIMPA, 506, 250.

[9] Bernard, D. 2018, NIMPA, 899, 85.

[10] Atwood, W., Albert, A., Baldini, L., et al. 2013, arXiv:1303.3514.